SLAC-PUB-6127
April 1993
(M)

Status of the Stanford Linear Collider*

JOHN T. SEEMAN
Stanford Linear Accelerator Center, Stanford University
Stanford, California, 94309 USA

ABSTRACT

The Stanford Linear Collider (SLC) was built to collide single bunches of electrons and positrons head-on at a single interaction point with single beam energies up to 55 GeV. The small beam sizes and high currents required for high luminosity operation have significantly pushed traditional beam quality limits. The Polarized Electron Source produces about 8 x 10^{10} electrons in each of two bunches with up to 28% polarization. The Damping Rings provide coupled invariant emittances of 1.8 x 10^{-5} r-m with 4.5 x 10^{10} particles per bunch. The 57 GeV Linac has successfully accelerated over 3 x 10^{10} particles with design invariant emittances of 3 x 10^{-5} r-m. Both longitudinal and transverse wakefields affect strongly the trajectory and emittance corrections used for operations. The Arc systems routinely transport decoupled and betatron matched beams. In the Final Focus, the beams are chromatically corrected and demagnified producing spot sizes of 1.7 to 2.2 μm at the focal point. Spot sizes below 1.7 μm have been made during special tests. Instrumentation and feedback systems are well advanced, providing continuous beam monitoring and pulse-by-pulse control. A luminosity of 2.3 x 10^{29} $cm^{-2}sec^{-1}$ has been produced. Over 11,000 polarized Zs were recorded in the SLD detector in the 1992 physics run.

* Work supported by the Department of Energy, contract DE-AC03-76SF00515.

Invited Talk at the ECFA Workshop on e+e- Linear Colliders (LC92)
Garmisch-Partenkirchen, Germany, July 25 - August 2, 1992.

1. Introduction

The SLC[1,2], the first linear electron-positron collider, was built at the Stanford Linear Accelerator Center (SLAC) to study the leptonic and hadronic decays of the Z^0 boson near a center of mass energy of 91 GeV. This collider was built inexpensively by using as a basis the existing two mile accelerating structure, albeit with many modifications and additions from beginning to end. During the design and commissioning of the SLC numerous advances in accelerator physics and beam diagnostics of high energy, high brightness beams have been made. These advances have applications not only for the next generation of linear collider but also for synchrotron radiation sources, free electron lasers, high brightness beam sources, and ultra-low emittance storage rings. Some of the issues being explored include very small emittance bunches, beams of extremely high power densities, multiple bunch beams, beam-beam interaction, positron target design, polarized electron gun design, low emittance damping rings, wakefield compensation, chromatic correction, halo collimation, reliability, instrumentation, and controls.

The usefulness of a collider is gauged by the time integrated luminosity with conditions acceptable for the physics detector at the interaction point (IP). The luminosity L of the SLC can be calculated from the parameters of the beams.

$$L = N^+ N^- f / (4 \pi \sigma_x \sigma_y) \qquad (1)$$

where N^+ is the average number of positrons per bunch, N^- is the corresponding number of electrons, f is the collision rate, and σ_x and σ_y are the horizontal and vertical transverse beam sizes at the IP, respectively. The bunch size is determined by the emittance ε of the beam and the betatron function β. $\sigma = [\varepsilon \beta]^{1/2}$. The emittances throughout the SLC are usually stated in energy invariant units (normalized) given by $\gamma\varepsilon$, where γ is the relativistic energy factor E/mc^2.

The normal collision cycle for the SLC is illustrated with Fig. 1. A positron bunch and two electron bunches are extracted from their respective damping rings. The positron bunch and the first electron bunch are accelerated to 47 GeV/c^2 in the SLAC linac with a gradient of about 18 MeV/m. After they pass through the two arcs and are reduced to a small size by the final focus system, they are collided at the IP. The spent beams are discarded after a single collision. On the same acceleration cycle, the second electron bunch after being accelerated to about 30 GeV in the linac (2 km) is extracted and made to strike a water cooled tungsten target. Positrons emerge from the target with energies near 1 MeV/c. The positrons are carefully collected while being accelerated to 200 MeV/c^2. They are then transported to the beginning of the linac in a quadrupole lattice (2 km). Upon the arrival of the positron bunch, the first section of the linac (100 m) is pulsed with radio-frequency (RF) power and used to accelerate the positron and two new electron bunches, which are made by either a thermionic or a polarized electron gun. These bunches are injected into the two 1.15 GeV damping rings, where radiation damping reduces the emittances to values required for small beam sizes at the final focus. Throughout this cycle a second positron bunch has remained in the positron damping ring, where two damping cycles are required to reduce its naturally large initial emittance. This complete cycle is repeated at 120 Hz.

The inherent instabilities of linacs in general have been compensated in the SLC by the use of slow (one minute) and fast (every pulse) feedback systems, all of which are computer driven. Nearly 100 measured beam parameters are actively controlled. In the spring of 1991 the SLD detector[3] was installed in the interaction region.

Selected design parameters of the SLC are listed in Table 1. Also included in Table 1 are the best individually achieved parameter values (while not maintaining the others), the simultaneously achieved values during initial SLD data collection, and the goals for the 1992 run[4]. The scales of beam parameters over the project is quite large. Here are two examples. Milli-electron-volts are discussed for issues within the photo-cathode of the polarized electron source as compared to 50 giga-electron-volt particles in the final focus. Beam diameters of a few microns are important in the final focus as contrasted with 10 centimeter diameters in the positron return line.

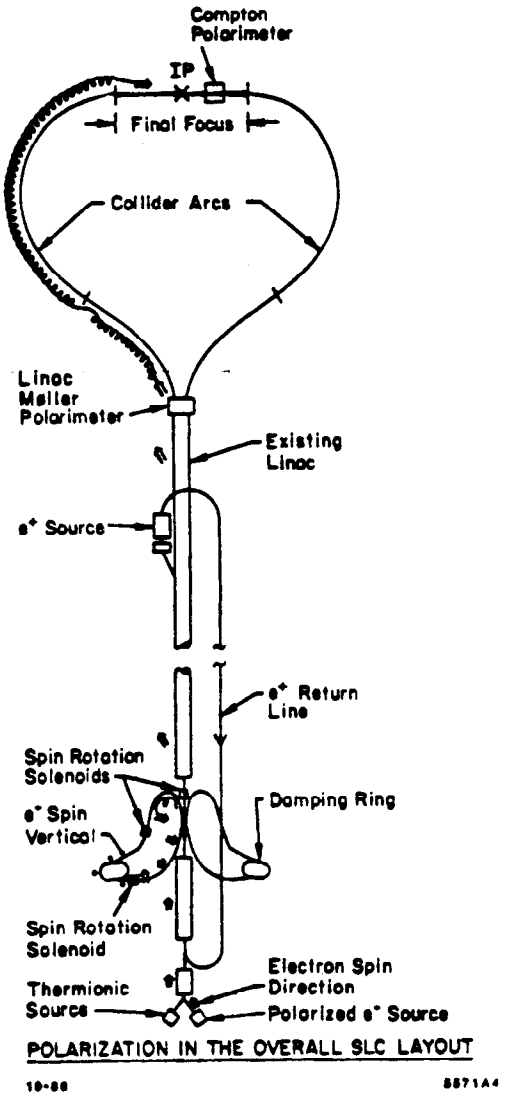

Fig. 1 A schematic overview of the Stanford Linear Collider (SLC). The length is 4 km.

Table 1 SLC Accelerator Parameters in August 1992

Accelerator Parameter	Units	1984 Design	Best Independently Achieved	Simultaneous during 1992 SLD Collisions	Goal for 1992 SLD Collisions
Beam energy	GeV	50	53	46.6	46.6
Repetition rate	Hz	180	120	120	120
Energy spectrum	%	0.25	0.2	0.33	0.3
N^- at IP	10^{10}	7.2	3.5	3.1	4.0
N^+ at IP	10^{10}	7.2	3.2	3.0	4.0
N^- in Linac	10^{10}	7.2	4.8	3.3	4.5
N^+ in Linac	10^{10}	7.2	3.8	3.2	4.5
N^- (210 MeV)	10^{10}	8.0	7.0	5.0	8.0
N^+ (210 MeV)	10^{10}	14.0	10.0	8.0	10.0
e^+ yield	e^+ / e^-	1.0	1.3	1.1	1.1
$\gamma\varepsilon^+_{x(y)}$ in Linac	10^{-5} r-m	3.0 (3.0)	2.0 (2.0)	4.0 (3.5)	3.0 (3.0)
$\gamma\varepsilon^-_{x(y)}$ in Linac	10^{-5} r-m	3.0 (3.0)	2.1 (2.0)	3.7 (3.5)	3.0 (3.0)
IP beam divergence	μrad	300	400	300	300
IP beam size σ for x	μm	2.07	1.7	2.2	1.8
IP beam size σ for y	μm	1.65	1.4	1.7	1.8
Bunch length (σ_z)	mm	0.5-1.5	0.5-12.	1.1	1.2
Pinch enhancement		2.2	1.05	1.05	1.1
Peak luminosity	$10^{29}/cm^2sec$	60.	2.3	2.3	4.5
Peak luminosity	(Z_{eff} / hour)	625	25.	25.	47.
Peak integrated luminosity	(Z^0 / day)	15000	350	350	500
Efficiency (accelerator)	%	100	90	60	50
Electron polarization (IP)	%	39	27	25	34
Cathode Quantum Efficiency	%	4	11	8	4

2. Polarized Electron Source

A polarized electron source[5,6] with a bulk GaAs photo-cathode was installed in spring 1992 to provide longitudinally polarized electrons at the IP. A schematic diagram of this gun is shown in Fig. 2. All components of the gun system were commissioned and produced good results for the initial polarized SLD physics run[7]. A bunch charge of 8 x 10^{10} e^- per pulse in each of the two bunches was achieved. A maximum polarization of about 28% was observed.

Downstream of the polarized gun, the two electron bunches are handled exactly the same as unpolarized bunches with the exception of injection and extraction from the electron damping ring. The transport line from the linac to the damping ring is designed to have the proper energy and spin precession angle so that a superconducting solenoid (6.4 Tesla-meter) located in that line rotates the longitudinal spin from the gun into the vertical direction for injection into the ring. The vertical spin remains polarized during the damping cycle if care is taken to avoid depolarizing resonances. On extraction, the bunches pass through two similar solenoids, one in the ring-to-linac transport line and the other in the early linac. These solenoids are used to align the spin in the precise orientation to make longitudinally polarized electrons at the IP after many precession cycles, both horizontally and vertically, in the SLC Arcs. Measurements have shown that with present SLC parameters both solenoids are needed to make longitudinally polarized electrons at the IP. The number of vertical spin rotations in the Arcs is strongly dependent on the vertical trajectory. Thus, the trajectory in the Arcs must be controlled with a feedback system. Typical longitudinal polarization values at the IP are 20-25%.

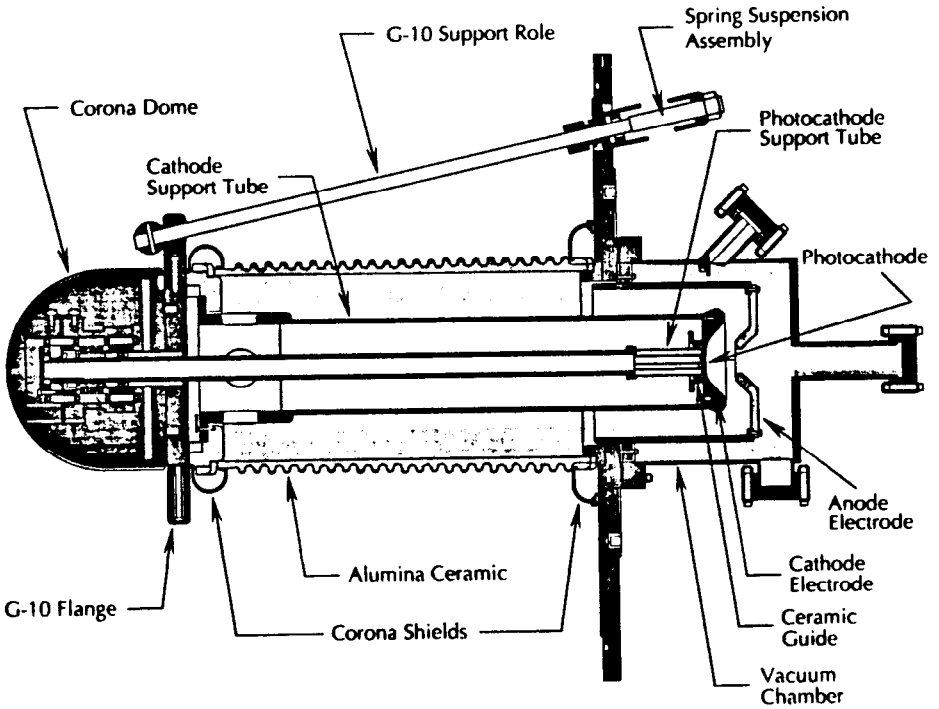

Fig. 2 Schematic diagram of the polarized electron gun at the SLC.

The polarized gun is activated by a heat treatment followed by the application of an atomic layer of cesium. This treatment must be repeated periodically to restore the quantum efficiency. A computer recorded history of these treatments over the first running period April 18 to May 21, 1992, is shown in Fig. 3 illustrating the quantum efficiency as a function of time[7]. A re-cesiation occurred at each large upward step. A heat treatment of the cathode was done on May 6. Note that the rate of decay of quantum efficiency increases with each re-cesiation but that a heat treatment restores the initial rate. Also, the maximum quantum efficiency grows with time. Furthermore, during tests of the polarized gun in the fall of 1991, an unexpected charge limit with laser light intensity relating to the quantum efficiency was discovered[7]. This effect reduces the charge obtainable in both bunches. The relevant surface physics effects which describe these phenomena are under active debate.

Apart from the polarized gun, the entire electron injector (gun, buncher, and 1 GeV linac) was developed to transport high charge, multiple electron bunches from the gun to the damping ring while maintaining reasonable emittances, good energy spreads, and equal energies. Most of these goals have been achieved but parameter stability from second-to-second and from day-to-day has been troublesome. The stability of the injector has been significantly improved through reproducible accelerator parameter configurations which remain appropriate for weeks. One particular problem has been the emittance of the high charge electron beam at the entrance to the damping ring. Often it is too large, causing particle loss and larger than expected beam emittance on extraction from the ring. This enlarged emittance has been traced to transverse wakefields in the early accelerating structures of the injector (30 to 200 MeV) and to injection mismatches. The wakefield effect has been mostly ameliorated by the addition of a betatron oscillation to the beam at the appropriate betatron phase over the later two thirds of the injector (80 m). This oscillation produces an additional wakefield beam tail which cancels the unknown wakefield effects. More information on these canceling oscillations is given in the Linac section. With these corrections, 5.6 x 10^{10} e^- in one bunch and 4.7 x 10^{10} e^- in each of two bunches (4 x 10^{10} is routine) have been extracted from the e^- ring.

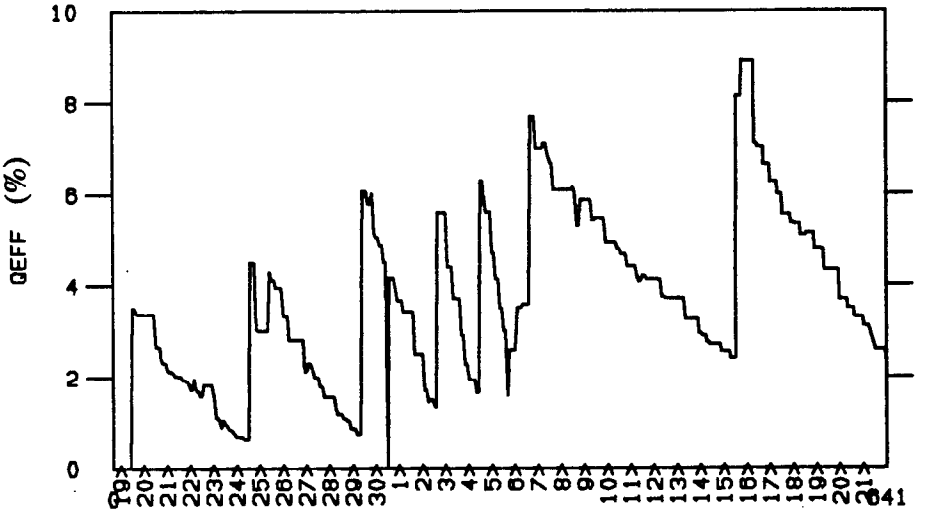

Fig. 3 Measured quantum efficiency of the polarized electron source for the first month.

3. Damping Rings

The damping rings of the SLC have been designed to reduce rapidly the transverse emittance of two bunches spaced nearly equally around the 35-m circumference. In order to make the damping time short compared to the beam cycle time, the horizontal betatron tune ($\nu = 8.3$) was made very high compared with a normal storage ring of that size. The ring is operated on the coupling resonance to make the horizontal and vertical emittances equal. The bunches are injected on axis into the ring using a kicker with fast rise and fall times (60 nsec). The extraction kicker removes the bunches in a single pass and must have amplitude stability at the 0.05% level to avoid transverse wakefield effects in the beams along the linac. Both rings have been operated successfully and routinely. Several problems appear at high bunch charges. Three phenomena stand out: 1) a longitudinal π mode instability develops above about 3×10^{10} particles per bunch, (2) a bunch length instability (relaxation oscillation) appears above about 2.8×10^{10}, and 3) the horizontal emittance does not damp to the desired value for 120 Hz operation.

The observed longitudinal π mode instability causes phase oscillations in the two bunches in the ring[8]. These phase oscillations result in unwanted random trajectory changes upon extraction where there is finite dispersion leading to unwanted emittance growth downstream. The instability depends upon the RF cavity temperature and tuner positions. At high currents the π mode instability is very sensitive to these parameters and is difficult to control. An idling feedback cavity has been installed to reduce this unwanted effect and has been shown to work effectively[8]. In addition, longitudinal feedback for the π mode has been tried using signals from the two bunches separately. The initial results are promising but further work is needed.

A spontaneous bunch length oscillation (single bunch) appears above about 2.8×10^{10} particles per bunch. After injection the bunch length damps naturally due to synchrotron radiation. At a certain reduced bunch length, the instability is triggered and the length increases rapidly (10%) over a few synchrotron oscillation cycles. The growth then stops and again synchrotron radiation starts to reduce the length. This relaxation repeats several times over the 8.3 msec storage time. For long storage times the oscillations eventually stop as an equilibrium is reached at a longer length. These oscillations affect downstream beam quality where the bunch length changes drive wakefield effects. Many studies have been performed to find a cure. A partial cure has been to ramp the RF amplitude down after the beam has been injected and then to ramp back to full value immediately before extraction, thus increasing the average bunch length. This ramp complicates the bunch length compression downstream and causes other longitudinal problems (e.g. Robinson's instability) during the period of low RF voltage.

At long storage times (1/60 second) of the bunches in the ring, the extracted emittances have been measured to be equal to the design equilibrium values if the ring is correctly aligned. With small misalignments of the ring girders so that the equilibrium orbit is displaced horizontally (1 mm or so) in the ring quadrupoles, the damping partition numbers (J_x and J_e) can change about 10%. Thus, the equilibrium emittance and the damping times can change on that order. At shorter storage times (namely 1/120 second needed for 120 Hz operation), these partition number changes lead to enlarged extracted

emittances. The electrons are more sensitive than the positrons as the positron bunches are stored for two damping cycles each. A measurement of the beam emittance as a function of the storage time in the ring is shown in Fig. 4. The measured damping time is 3.9 msec, as compared to the design time of 3.6 msec. The equilibrium emittances are about 1.8 x 10^{-5} rm, also about 10% high. The alignment of each ring is checked periodically as the tunnel floor creeps with time. A related ring parameter which has been shown (unexpectedly) to affect the damping is the horizontal tune, which is illustrated in Fig. 5. A new operating point with a horizontal tune of 8.28, increased from the nominal 8.17, has successfully reduced the extracted emittances[9]. It is also important to maintain small injected emittances.

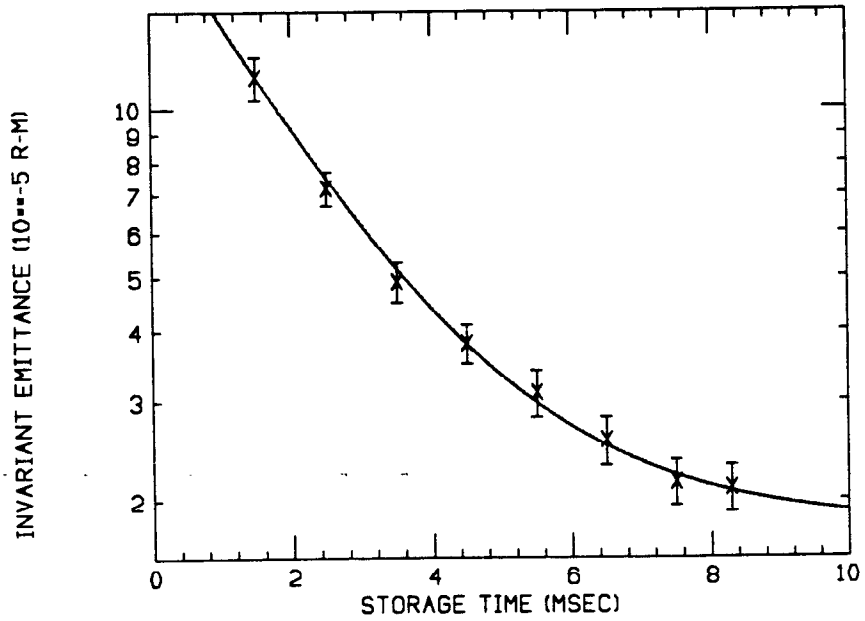

Fig. 4 Measured extracted emittance versus storage time in the electron damping ring.

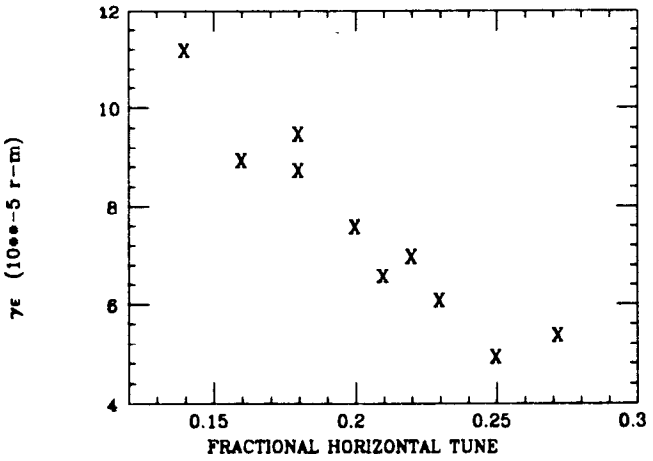

Fig. 5 Measured extracted emittance versus the horizontal betatron tune at 5.6 msec.

4. Bunch Length Compressor

In the transport line between the damping ring and the linac, the bunch length is shortened from 6-9 mm to 1 mm. This shortening is done by introducing a head-tail energy difference along the bunch and passing the beam through a non-isochronous bend. $\Delta z = R_{56} \Delta E/E$. This process is schematically shown in Fig. 6. Several emittance enlargement effects may occur in this region, mostly are related to the large energy spread[10].

Betatron mismatches[11] occur when the injected beam has a phase-space orientation (β,α) that does not match the linac lattice. This mismatch is illustrated in Fig. 7. Because of the nature of the chromatic linac lattice, particles with different energies have different betatron oscillation frequencies. Thus, they rotate in phase space at different rates, and soon the bunch undergoes filamentation. Given beam Twiss parameters β_b and α_b that are mismatched from the lattice design values β_l and α_l, the emittance enlargement after filamentation is given by a parameter Bmag.

$$(\gamma\varepsilon)_{final} = \text{Bmag} \cdot (\gamma\varepsilon)_{initial} \tag{2}$$

with

$$\text{Bmag} = \frac{1}{2}\left[\frac{\beta_l}{\beta_b} + \frac{\beta_b}{\beta_l} + \beta_b \beta_l \left(\frac{\alpha_b}{\beta_b} - \frac{\alpha_l}{\beta_l}\right)^2\right] \tag{3}$$

To avoid emittance increases of order 10%, β_b must be matched to about 30%. The α_b match has a similar constraint. These matches are relatively straight forward in practice.

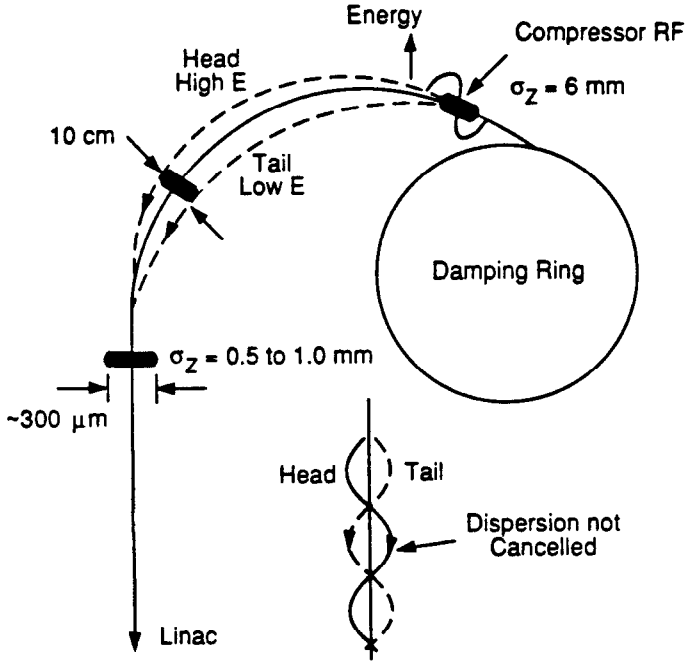

Fig. 6 An overview of the ring-to-linac transport line showing bunch length compression.

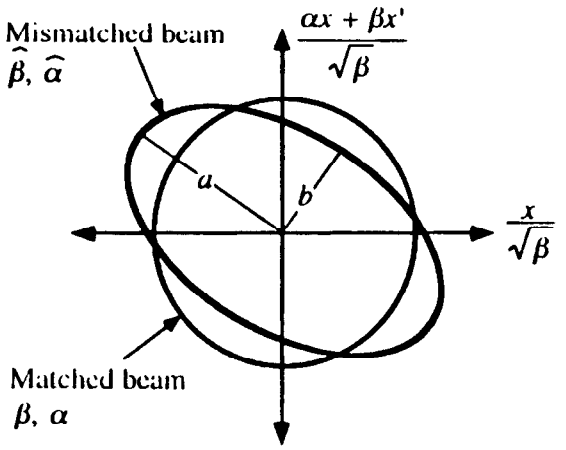

Fig. 7 Filamentation of a betatron mismatch of the beam. The mismatch is quantified by half the sum of squares of the major and minor axes[11].

Any anomalous dispersion η (η') present in the beam produces a transverse position-energy correlation which adds to the apparent size and emittance of the beam: $\sigma^2 = \varepsilon\beta + \eta^2\delta^2$. If β_1 and α_1 are the lattice Twiss parameters, then the measured effective emittance ε_{eff} in the presence of beam dispersion and energy spread δ is given by

$$\varepsilon_{eff}^2 = \varepsilon_\beta^2 + \frac{\varepsilon_\beta}{\beta_1}\left[\eta^2 + \left(\beta_1\eta' + \alpha_1\eta\right)^2\right]\left\langle\delta^2\right\rangle \tag{4}$$

With filamentation along the linac the emittance increases further leading to a final value of

$$\varepsilon_{eff} = \varepsilon_\beta + \frac{1}{2\beta_1}\left[\eta^2 + \left(\beta_1\eta' + \alpha_1\eta\right)^2\right]\left\langle\delta^2\right\rangle. \tag{5}$$

To make the increase in the emittance from dispersion negligible, dispersion errors at injection must be controlled to a few millimeters in the SLC. Minimization of the measured emittance early in the linac is performed by adjusting quadrupoles in the ring-to-linac transport line to adjust the dispersive transport elements (R_{16} and R_{26}).

The large energy spread in the beam ($\sigma_E/E = 1\%$) also allows errors in the second- and third-order transport to affect the emittance and betatron match[11]. The introduction of independent sextupole power supplies has provided a nearly complete set of second-order orthogonal dispersive controls (T_{166} and T_{266}) and betatron chromaticity adjustments (T_{116}, T_{126}, and T_{226}). The installation of two octupoles (10 cm length, 6.5 cm bore, and a pole tip field of 40 gauss) allows the correction of the third-order dispersive terms (U_{1666} and U_{2666}). For example, the optimization of emittance early in the linac as a function of the U_{1666} corrector strength is shown in Fig. 8. The optimization of the dispersion adjustments requires several hours to complete but remains stable for weeks. Nevertheless, after all these corrections have been made, a 30% increase in emittance at the beginning of the linac still occurs while increasing the bunch charge to 4×10^{10} particles. The increased emittance is definitely energy spread related due to the longer bunch lengths with increased currents. The expected errors are likely to be second-order chromatic terms, such as U_{1266}.

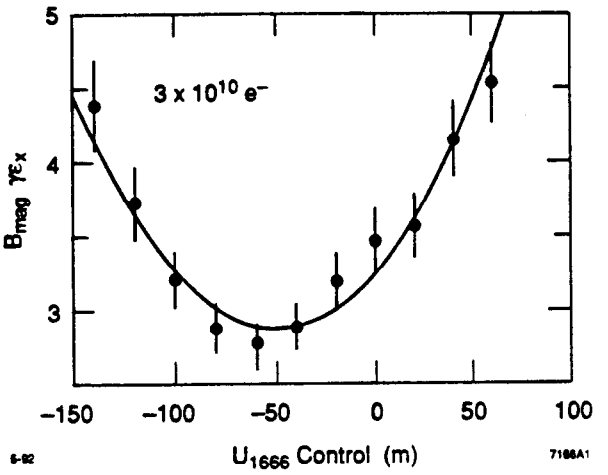

Fig. 8 Measured emittance at 1.15 GeV as a function of the U_{1666} control octupoles.

5. Linear Accelerator

The main linear accelerator (linac) at Stanford has a length of 2946 m and is powered by 230 klystrons each producing 67MW. The accelerating gradient after RF pulse compression is about 20 MeV/m. A strong focusing lattice of 282 quadrupoles is used to maintain the transverse beam size. A pair of x-y correction dipoles and a stripline position monitor ($\Delta x_{resolution}$ = 20μm) are associated with each quadrupole. Beam profile ($\Delta\sigma_{resolution}$ = 3 μm) and emittance measurements are made at the beginning, middle, and end of the linac.

The primary goal of the linac is to transform the six dimensional phase space volume of a low emittance, low energy bunch to high energy without significant phase-space enlargement. Acceleration by itself reduces the absolute emittance of the bunches by increasing the longitudinal velocities of the particles while leaving the transverse velocities constant. However, deleterious effects such as transverse wakefields, RF deflections, chromatic filamentation, and injection errors can increase the emittance, if allowed.

5.1 *Longitudinal effects*

The energy E of particles accelerated in the linac after n klystrons is given by

$$E(z) = E_{inj} + \sum_{i=1}^{n} [\, \Delta E_i \cos(\phi_i+\phi(z)) + \Delta s_i \int_z^{\infty} W_l(z'-z)\, \rho(z')\, dz'] \qquad (6)$$

where E_{inj} is the injection energy, ϕ_i are the klystron phases (which are free parameters), $\phi(z) = 2\pi z/\lambda_{RF}$, λ_{RF} is the RF wavelength, z is the longitudinal position along the bunch, ΔE_i is the maximum energy gain in the distance Δs_i (one klystron), $\rho(z)$ is the longitudinal density distribution, and the last term on the right-hand side is the longitudinal wakefield

contribution to the particle energy. The longitudinal wakefield contribution W_l arises from all particles in the bunch preceding the one of interest. The longitudinal wakefield depends on the shapes of the RF cavities and surrounding vacuum hardware. For the SLC ΔE_i = 20 MeV/m, λ_{RF} = 10 cm, and Δs_i = 12 m. $\rho(z)$ is a Gaussian distribution at low currents with σ_z = 1mm. At 5 x 10^{10} particles the longitudinal wakefield decelerates the tail by 2 GeV over the 3 km linac. Thus, in order to minimize the energy spread, the mean phase of the bunch is moved forward of the RF crest. The energy distribution in the bunch develops a complicated "double horned" shape due to the nonlinear wakefield, particle density distribution, and RF sine wave. The shift in the optimum linac phase for the minimum energy spread as a function of current can be up to 15 degrees. Furthermore, at high currents the longitudinal bunch distributions are not true Gaussians and a careful integral is required to extracted the energy spectra.

The SLC linac accelerates three bunches[12]. The long range longitudinal loading affects the energy differences between the bunches, as trailing bunches see a lower accelerating field. The energy extracted from the RF cavities by the beam must be replenished by the RF power source but there is a finite filling time. The method to equalize the bunch energies is to increase the klystron pulse amplitude with time using the pulsed SLED system.

5.2 *Transverse Effects*

A static launch error of the beam injected into the linac generates a betatron oscillation. Standard computer controlled trajectory correction is used to restore the proper launch. There are eight position-angle feedback systems distributed along the accelerator to keep the trajectory stable. However, if the launch of the beam fluctuates more rapidly than feedback can correct it, other methods of control are needed[13]. The transport equation of motion for particles in the bunch can be used to study oscillations along the linac.

$$\frac{d^2}{ds^2} x(z,s) + k^2(z,s)\, x(z,s) = \frac{r_e}{\gamma(z,s)} \int_z^{\infty} dz'\, \rho(z') W_r(z'-z)\, x(z',s), \qquad (7)$$

where s is the distance along the accelerator, z is the distance internally along the bunch, k is the quadrupole focusing term (which varies along the linac and along the bunch because of energy changes), ρ is the line density, W_r is the transverse wakefield due to the accelerating structure, and r_e is the classical electron radius. The left-hand side of Eq. 7 represents a betatron oscillation including (slow) acceleration. The right-hand side introduces the forces from transverse wakefields on each particle generated by position errors in the RF structure of all the preceding particles in the bunch. The transverse wakefields for the SLC structure increase in strength with the distance behind the leading particle. Thus, the particles at the back of the bunch, in general, see the largest forces. The displacements grow exponentially with distance along the linac. Several photographs of beam transverse enlargement at the end of the linac from betatron oscillations are shown in Fig. 9, indicating the strength of the effect after 30 betatron wavelengths.

Fig. 9 Profiles (x-y) of a 2 x 10^{10} e^- bunch at 47 GeV with a 0.2 mm oscillation (left), with a 0.5 mm oscillation (center), and with a 1 mm oscillation (right) in both planes. The initial core sizes in both planes are about 120 μm.

This strongly forced oscillation of the tail by the head (seen in Eq. 7) can be ameliorated by changing the energy spectrum along the bunch so that the head is higher in energy than the tail; this can be accomplished with RF phase adjustments. This technique to control the resonant growth is called BNS damping (named after the inventors: V. Balakin, A. Novokhatsky, and V. Smirnov)[14]. BNS damping lowers the energy of the back of the bunch by accelerating the bunch behind the crest of the RF early in the linac and then ahead of the RF crest downstream to restore the energy spread at the end. With the back of the bunch low in energy, the wakefield forces in Eq. 7, which act to defocus particles, are counterbalanced by the increased quadrupole focusing of the back of the bunch because of its low energy. The resonant excitation is then reduced if not arrested. It is not possible to perfectly cancel the forces over the whole bunch so some enlargement is expected. BNS damping has been studied at the SLC and has been shown to be so effective that all SLC linac operations now use it. The BNS settings used for SLC operations at 3 x 10^{10} particles have the first 56 klystrons phased at -20 degrees and the remaining klystrons phased at +15 degrees[15]. In all cases the overall linac phase is adjusted to make the energy spectrum small (about 0.3%) at the end of the accelerator. An observation of the effect of BNS damping is shown in Fig. 10. The effect of BNS damping on beam oscillations can be studied as a function of bunch charge. In Fig. 11 several bunch oscillations with identical initial conditions are shown along the linac as a function of charge. At low currents the bunch filaments rapidly with a large emittance increase. At about 1.5 x 10^{10} particles the bunch oscillation nearly follows that of a single adiabatically damped particle with the same oscillation. At higher charge the oscillation starts to grow at the end of the linac due to transverse wakefields. These growing oscillations indicate that the longitudinal tail of the beam is being driven farther and farther off axis as can be seen in the above beam profile measurements[16].

Misalignments of the quadrupoles, position monitors, and accelerating structures in the linac cause each beam (after correction) to have a trajectory that is neither straight nor centered in the accelerating structure. These offsets generate dispersion and wakefield emittance growth as described above. There are several methods to deal with these errors. (a) They can be found mechanically and fixed, although the required accuracy is well

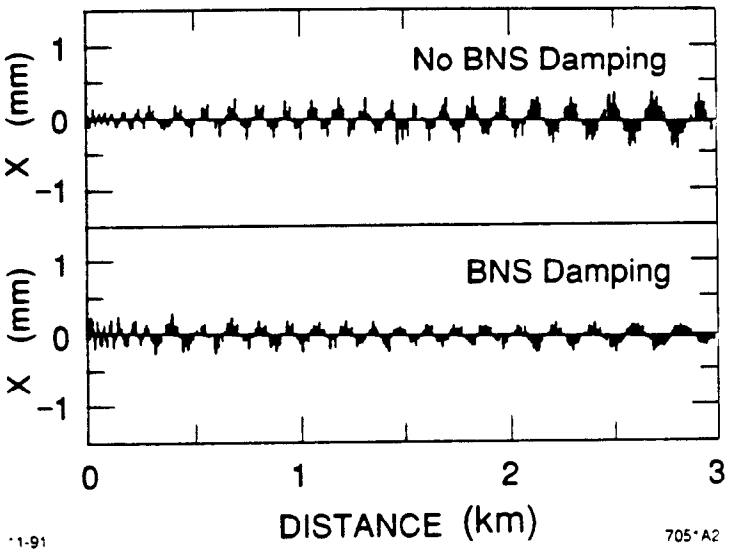

Fig. 10 Measured oscillations in the SLC linac with and without transverse wakefield damping (BNS). The bunch charges are 2 x 10^{10} e^-. The upper plot shows the exponential growth of the oscillation without BNS damping and the lower plot shows little growth with BNS damping. A factor of ten improvement is observed.

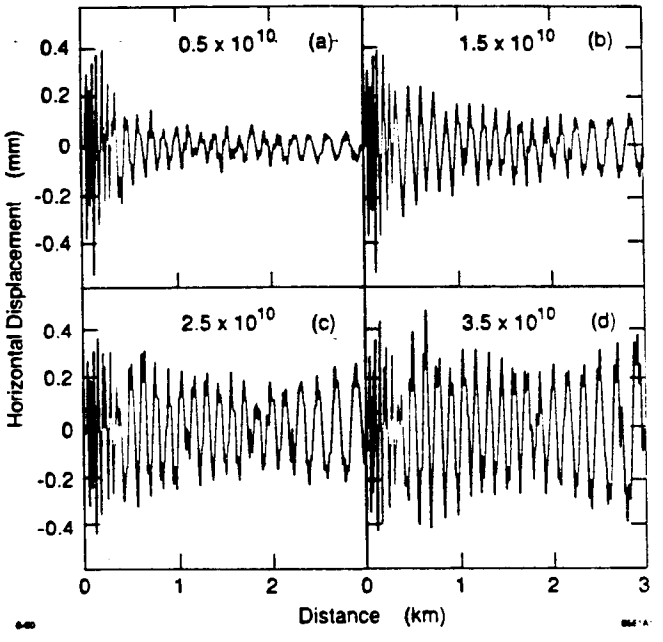

Fig. 11 Observed single bunch oscillations along the SLC linac versus charge for identical dipole changes. Standard BNS conditions for 3 x 10^{10} e^- are used in all cases with the overall linac phase adjusted to make a small energy spectrum at 47 GeV.

below 100 μm. (b) Calculations using knowledge of the beam trajectory as a function of the quadrupole lattice strength can determine the relative quadrupole and position monitor errors to about 75 to 100 μm. The misalignments can then be mechanically corrected. (c) A dispersion reducing trajectory correction may be tried. (d) Mechanical movers of the RF structure in the tunnel can be used in a betatron harmonic correction scheme to reduce the final emittance. (e) Betatron oscillations can be added to the beam at various locations along the linac to cancel effects of the existing absolute trajectory and thus minimize the final emittance. (f) Finally, harmonic changes can be added to the quadrupole lattice to cancel random and systematic errors in the quadrupole field strengths. The best combination of the available solutions depends on the particular errors involved. All have been tried on the SLC linac with various degrees of success[17]. Method (e) has been very successful.

At high currents after the input parameters are optimized and the trajectory nominally corrected, the primary emittance growth during acceleration arises from beam displacements in the accelerator components. These offsets result from the trajectory being steered through misaligned quadrupoles and accelerator structures onto beam position monitors with finite residual offset errors. Consequently, transverse wakefields excite the beam. Methods to reduce these effects have been theoretically studied[15]. It has been shown that the addition of appropriate injection errors (Δx, $\Delta x'$, Δy, and $\Delta y'$) can cancel most of the emittance enlargement. Since the advent of BNS damping, a more global scheme of distributing short range oscillations along the accelerator has been shown to be advantagous[10]. Examples of these oscillations are shown in Fig. 12. The emittance at full energy was measured as a function of the oscillation amplitude. The results are shown in Fig. 13. The $\gamma\varepsilon$ and $\gamma\varepsilon$ x Bmag measurements for the oscillation in Fig. 12a are shown in the left plot in Fig. 13. Both data curves track each other very well, indicating a completely filamented beam (Bmag=1). Furthermore, a decrease in the transverse emittance (25%) is observed with a finite oscillation added to the beam. The errors which caused the original emittance enlargement are thus likely to be near the beginning of the linac. For the oscillation of Fig. 12b, the invariant emittance (Fig. 13 right) at the end of the linac shows no reduction with oscillation amplitude. In addition, a large betatron mismatch has developed signaled by the separation of the curves for $\gamma\varepsilon$ and $\gamma\varepsilon$ x Bmag. A tail has grown.

Thus, the proper choice of the amplitude of a short range oscillation in the appropriate location can significantly reduce the emittance enlargement and preserve the betatron match[13,18]. In practice about ten short-range (200 m) oscillations in the SLC are applied to the two beams during collisions, reducing the emittances to near the design values at 3×10^{10} e^-. The trajectory offsets are about 200 μm and remain stable for days.

Feedback systems that work pulse-by-pulse are essential for keeping the beam parameters within acceptable limits given the many possible sources of transverse jitter: varying power supplies of dipoles and off axis quadrupoles, vibrating quadrupoles, klystron phase and amplitude jitter, unstable kicker magnets, and changes in the beam intensity. In the SLC, over 100 beam parameters (beam positions, angles, and energies) are controlled by feedback routinely with many corrections each second. Not all parameters need rapid feedback. For example, the energy spectrum feedback has proven not to need pulse-by-pulse control. Modern control theory is used to provide cascaded control of position and angle loops from the beginning to the end of the accelerator that minimally

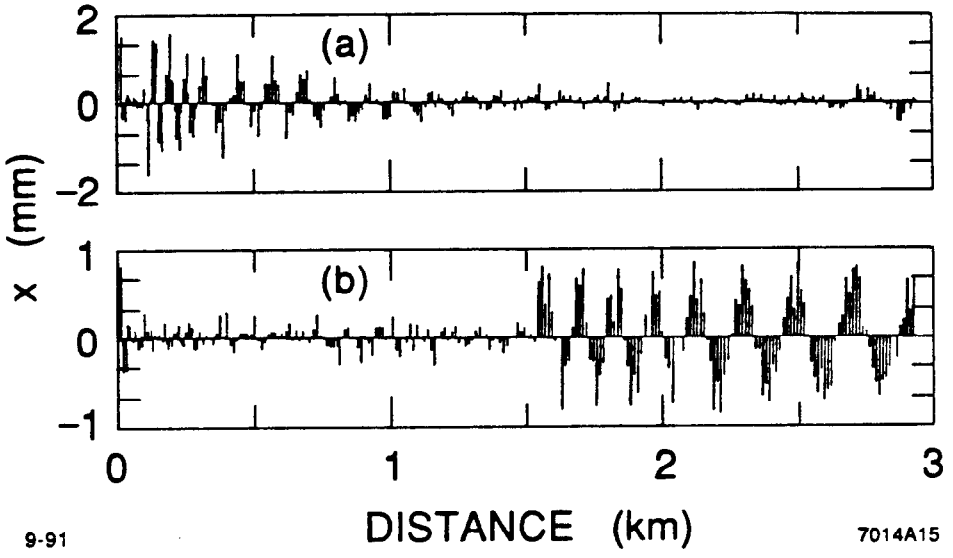

Fig. 12 Two typical induced oscillations in the SLC accelerator used to cancel accumulated wakefields and dispersion errors in the linac (see Fig. 13).

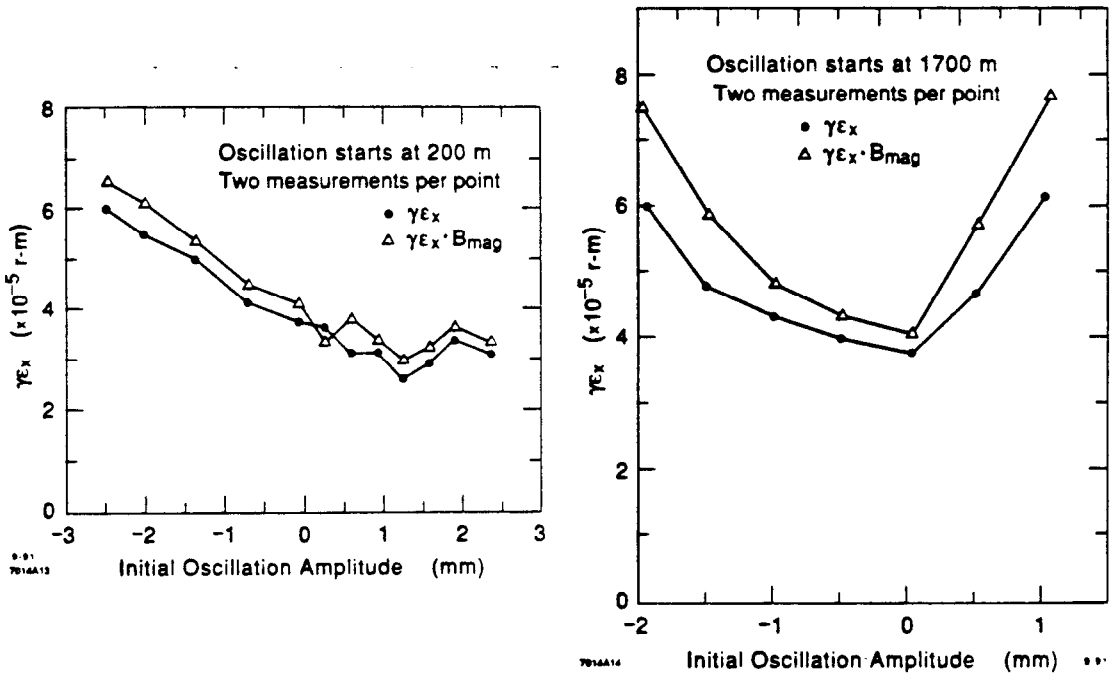

Fig. 13 Invariant emittance changes at the end of the linac (47 GeV) as a function of the amplitude of the oscillations shown in Fig. 12. The left data is for Fig. 12a, and the right data for Fig. 12b.

interfere with each other and provide maximum control[19]. A reduction of oscillation amplitudes with frequencies up to one sixth of the accelerator pulse rate can be expected.

One mechanism for substantial beam jitter with frequencies beyond the capabilities of feedback is the mechanical vibration of the quadrupoles. Studies have been made in the SLAC tunnel of the transverse vibration of the linac quadrupoles showing vibration frequencies of order 8 to 10 Hz, which is beyond the feedback frequency range. The amplitude of the observed oscillation depends on which of the two support schemes is used. The quadrupoles at the ends of the support girders with direct rigid supports to the tunnel floor show vibrations at the 0.05-μm level, which is adequate for the SLC. However, quadrupoles at the center of the long girders (12 m) show vibration levels up to 5 μm. The first 300 m region of the SLC linac has quadrupoles in the center of the girders as well as at the ends. Beam jitter resulting from these vibrating quadrupoles has been observed, as shown in Fig. 14. To fix this problem, mechanical struts to the wall and floor centered on these girders have been installed with a clamping arrangement compatible with normal mechanical alignment. These vibrations have thus been reduced to acceptable levels.

In a global view of the various regions of the SLC, many emittance enlargement effects have been eliminated. However, some have resisted complete cures and some are inherent in the design. A pictorial summary of the measured emittances along the SLC for the horizontal plane of the electron beam (the worst plane and beam) is shown in Fig. 15, indicating the sources of the emittance contributions. Lines have been added to separate the regions. These results are the culmination of work over several years. A summary of the emittance reduction work over that period is shown in Fig. 16. Significant progress has occurred. Present operation uses three bunches (e+, e-, e- scavenger) with charges up to 3 x 10^{10} particles per bunch. Emittance reduction techniques for higher currents are now under active study as intensities near 4.5 x 10^{10} are needed for collisions in the near future.

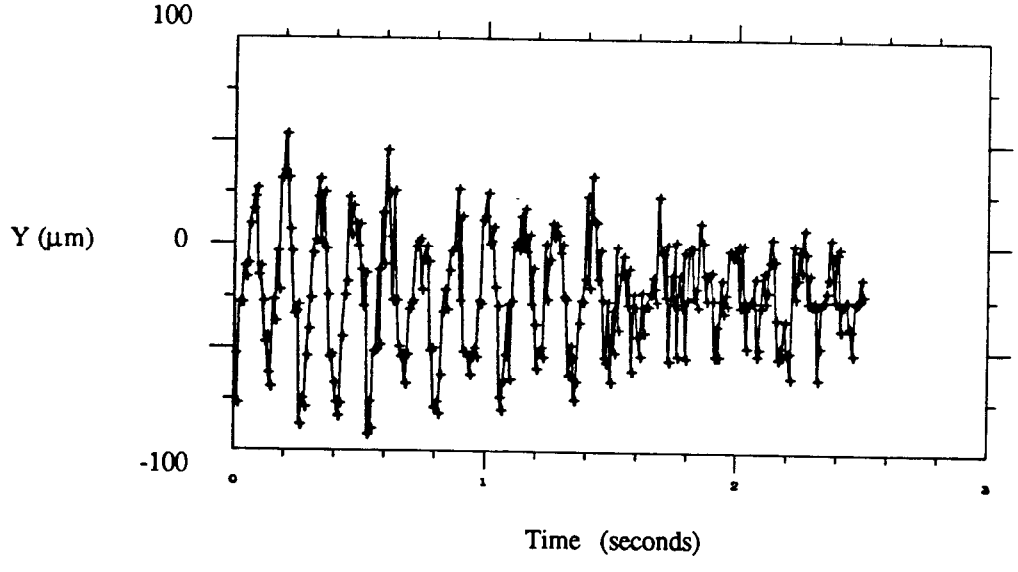

Fig. 14 Observed motion in the positron beam with time from vibrating quadrupoles. The amplitude change is from several beating frequencies. β = 20 m. E = 3 GeV.

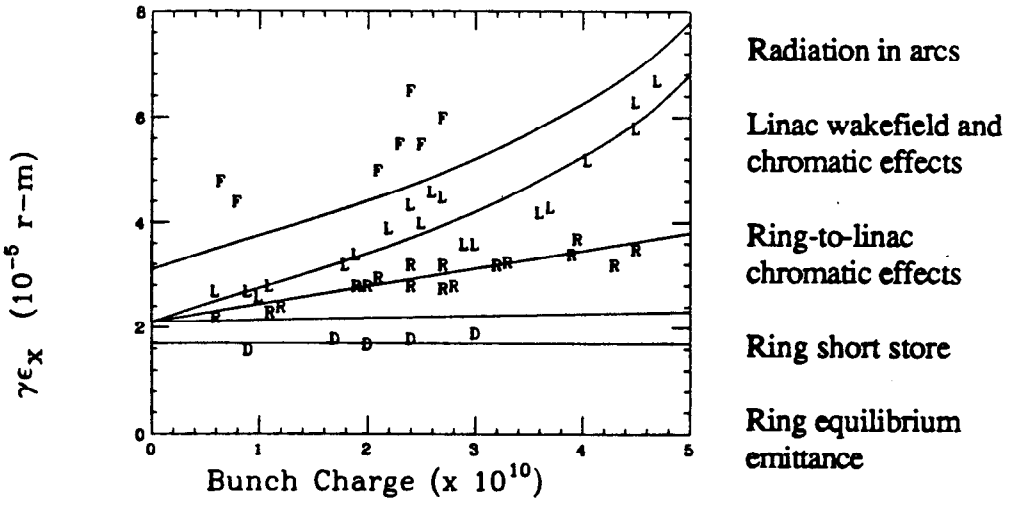

Fig. 15 Measured $\gamma\,\varepsilon_x$ versus e^- charge showing enlargement effects from the damping ring to the final focus. D represents measurements at the ring exit, R = linac entrance, L = linac exit, and F = final focus. The lines separate the various effects. The final focus measurements suggest that an additional ε growth effect is present.

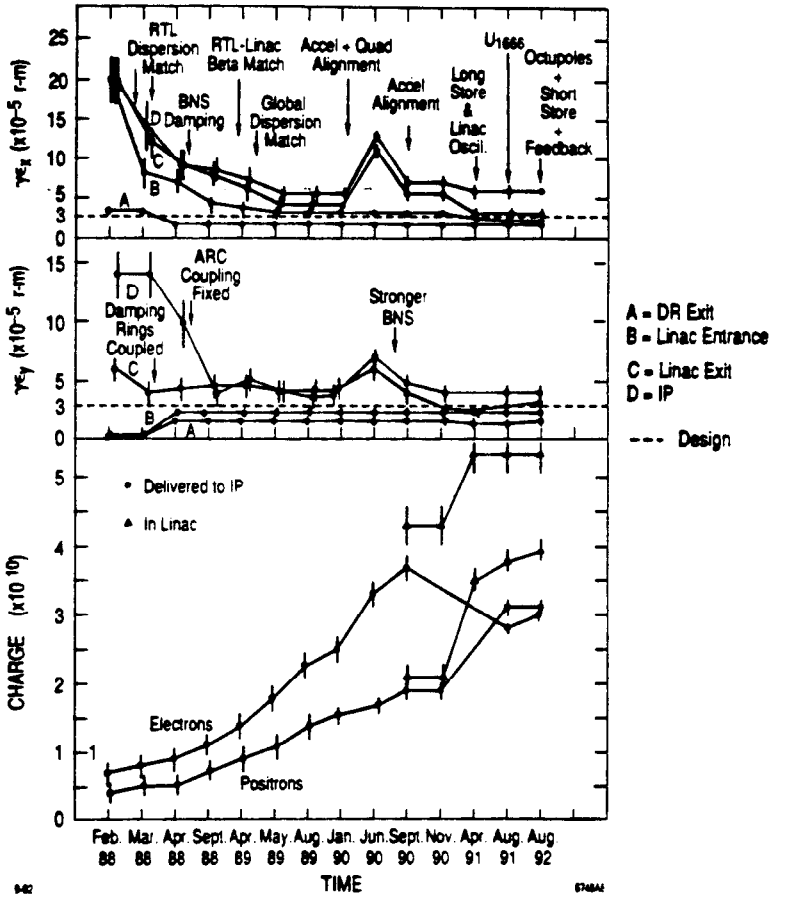

Fig. 16 Time evolution of the SLC beam emittances and intensities.

6. Arcs

The arcs must transport two high energy bunches from the linac to the final focus without significant emittance dilution. The arc system is comprised of a short matching region at the end of the linac leading into a very strong focusing FODO array of combined function magnets including dipole, quadrupole, and sextupole fields. Each lattice cell has a betatron phase advance of 108 degrees and a length of 5 m. Each 47 GeV particle loses about 1 GeV to synchrotron radiation in a single pass through the system. Ten pairs of magnets form a second-order achromat that can safely transport beams with an energy spectrum of 0.5%. There are 23 achromats in the north Arc, and 22 in the south. At the end of each F [D] magnet within an achromat a beam position monitor is attached to sense the x [y] beam position with an accuracy of about 25 mm. The combined function magnets are moved by motorized jacks for beam steering.

Achromat units (20 magnets) as groups are rotated around the beam axis up to 10 degrees to provide the needed vertical bending for terrain following. Initial matching problems and slight phase advance errors over the length of the achromats caused unwanted coupling of vertical and horizontal beam motion at the roll boundaries. Also, magnet misalignments contribute to unwanted emittance enlargements. A collection of several cures has now produced acceptable solutions. Tapered rolls at the achromat boundaries, betatron phase corrections using backleg coils on the magnets, trajectory steering by magnet movers, harmonic corrections at certain spatial frequencies, and 3π trajectory bumps for skew correction are all applied where needed along the arcs. These corrections are made after exhaustive oscillation data are taken throughout the arcs starting in the linac. A measure of these corrections is given by a parameter DetC which is the determinate of the measured off-diagonal transport matrix[20]. DetC is determined from the measured first-order transport matrix R_{ij}. A DetC measurement along the north arc is shown in Fig. 17 before and after corrections have been made.

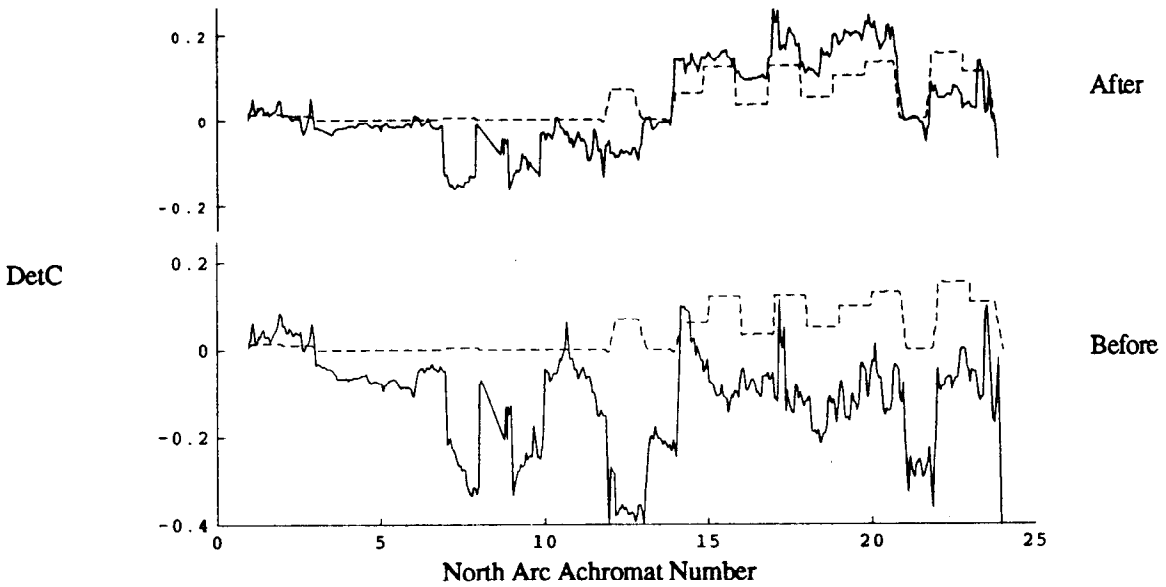

Fig. 17 Measured DetC before and after correctrion. The dashed line is the design.

7. Final Focus

The final focus system of the SLC must focus the two opposing beams to small sizes at the collision point and must steer the two beams into head on collision. A schematic view of the final focus[21] is shown in Fig. 18. The beam entering the final focus first encounters a correction region to remove dispersion entering from upstream. Then the beam passes through the first demagnifying telescope where the x and y planes have demagnifications of 8.5 and 3.1, respectively. Betatron mismatches and x-y coupling arriving from upstream are also corrected in this region. Next, the chromatic correction section (CCS), which contains gentle bends and sextupoles, is used to correct the trajectories of different energy particles so that they focus at the same longitudinal position at the interaction point (IP). The final telescope provides the last demagnification to make the smallest spots possible and to make the vertical and horizontal spots have equal size. After passing through the IP, each beam traverses through the opposing beam's transport line and is deflected into an extraction line to a high power dump. New superconducting quadrupoles have been installed as the final triplet along with the SLD detector. These quadrupoles are closer to the IP than the old conventional quadrupoles, allowing a reduced β^* and a doubling of the potential luminosity.

The minimum spot sizes at the IP depend on the incoming beam emittances, the maximum allowed divergence angles at the IP, chromatic corrections, and beam errors such as dispersion. The design values for the incoming beam emittances ($\gamma\epsilon$) are 4.5×10^{-5} r-m horizontally and 3.5×10^{-5} r-m vertically. However, during current operation the actual emittances are about 15% higher. The angular divergence is limited by backgrounds from synchrotron radiation in the strong focusing quadrupoles near the IP. Masking near the detector improves significantly the effects of this radiation. The angular divergence is limited to about 300 μrad for the SLD. Finally, the chromatic and geometric corrections are made by adjusting the sextupole strengths and installing offset trajectories in the sextupoles, thus minimizing the unwanted first-, second-, and third-order transport

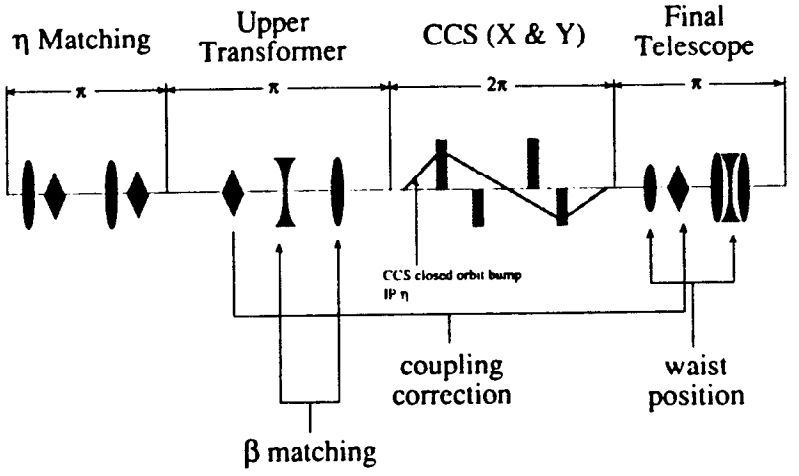

Fig. 18 Schematic view of the SLC Final Focus System indicating tuning regions.

elements. A plot of the expected spot sizes versus angular divergence[22] is shown in Fig. 19. From linear optics $\sigma^*_y = \varepsilon / \theta^*$. Therefore, the increase in spot size at low θ^* follows linear optics; but the rise at large θ^* is from higher order terms. Note that the spot size minima for both planes can be reached with $\theta^* = 300$ μrad.

The beams are very dense at the collision point and can exert large transverse forces on each other, referred to as beam-beam deflections[23]. As the two beams are steered through each other, the beam-beam deflection first adds and then subtracts from the bending angle. Several examples of measured beam-beam deflections are shown in Fig. 20. Beam-beam deflections can be measured in the horizontal, vertical, and skew planes. From the observed deflections, many beam properties can be derived. The beam centroid offsets are determined from the place where the deflection crosses zero. This offset is removed by using nearby dipole magnets to bring the beams into head on collision. The shape of the deflection curve indicates the size of the combined two-beam system and is a good indicator when upstream components have changed the beam parameters. Non-Gaussian transverse profiles of the beams can affect the beam-beam scans as can be seen in Fig. 20. Efforts are underway to maximize the information extracted from the beam-beam deflections[24]. Finally, jitter in the deflection measurements often indicates pulse-by-pulse position changes. Present jitter in the SLC is about one third of the beam size at the IP and results in only a small loss in average luminosity. A pulse-by-pulse feedback system using these signals keeps the beams in collision.

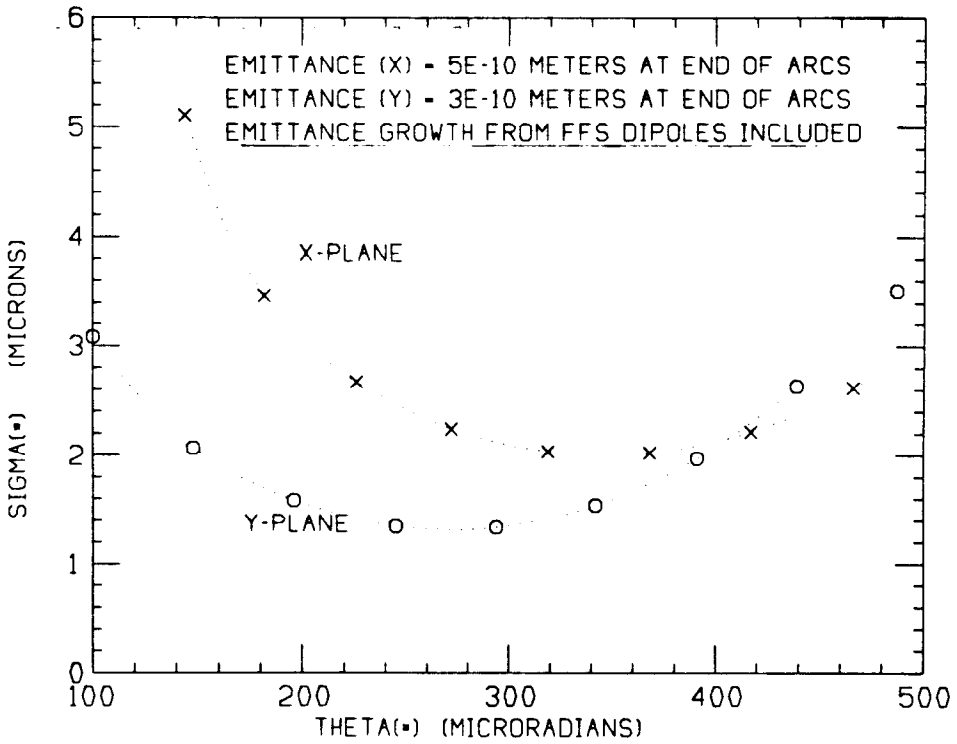

Fig. 19 Beam sizes at the interaction point as a function of beam angular divergence.

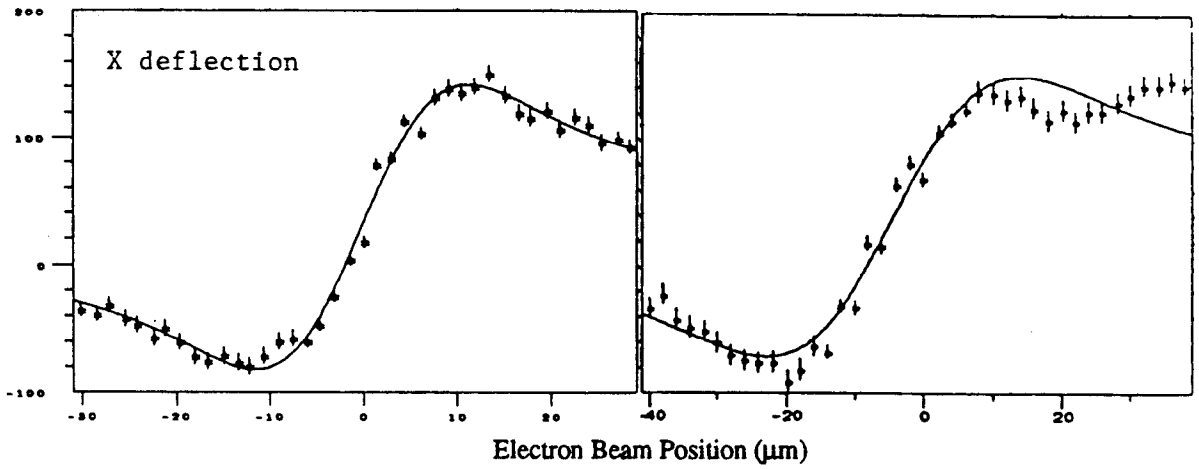

Fig. 20 Observed beam-beam deflections at the SLC Final Focus for about 2.5 x 10^{10} particles per bunch. The left data are for symmetrical beam profiles and the right data are for beams with non-Gaussian transverse tails.

The particles bent in the beam-beam interaction radiate a form of synchrotron radiation called "beamstrahlung". This radiation travels forward and is detected using a gas Cerenkov detector about 40 m downstream. The radiation from one beam is most intense where the particle density of the other beam is changing most rapidly, at about one transverse beam sigma. The integrated signal over the bunch can be measured as the beams are steered through each other. The signal shape can have a single peak or two peaks, depending on the initial sizes of the two beams[23]. The beamstrahlung signal can be displayed in real time and is a good indicator of instantaneous luminosity.

Recently, most of the studies in the final focus have been directed towards developing tuning algorithms for making small beam sizes and for tracking accelerator changes. In practice, the art of spot size minimization presents a challenge because of limited beam provided knowledge. Information from the beam-beam deflections represents integrals over both transverse beam distributions. Unraveling which beam and which beam parameter are the sources of the error requires subtle deconvolutions[24].

Additional information can be obtained with single beam studies. Single beams can be focused onto 4 μm diameter wires in profile scanners 20 cm from the IP. These studies can only be performed at low currents (< 1 x 10^{10}) because of wire breakage on single pulses. Extrapolating the results 20 cm to the IP and raising the bunch charge to running values bring new accelerator physics effects into play. This inability to measure the size of a single beam at high currents slows the tuning procedure for making small spots. For example, the match of the betatron function at the IP using beam-beam deflections is very hard if the incoming betatron mismatch is large. Also, to complicate matters, non-linear dispersion has been observed on occasion in the positron beam as it enters the final focus appearing as a horseshoe shaped x-y distribution, causing indecipherable beam-beam scans. Furthermore, the correction of this nonlinear dispersion effect must be made not only in the final focus but also upstream in the arcs.

8. Detector Backgrounds

The backgrounds in the SLD detector come from lost beam particles, synchrotron radiation of the beam in the strong IP quadrupoles near the detector, and beam-gas scattering[25]. The lost particles produce both muons emanating from upstream collimators and energetic electro-magnetic debris for strikes near the IP. The synchrotron X-rays often speckle the detector drift chamber displays with single hits. A good IP vacuum eliminates most beam-gas scatters.

Several arrays of collimators for background control are placed in the SLC as shown in Fig. 21. Eight x-y collimator pairs are placed at the end of the linac. The first four provide primary betatron cuts for particles greater than about 3 transverse beam sigma. About 10% of the total beam particles are lost in this cut. The second four collimator pairs at the end of the linac provide secondary betatron collimation and eliminates the particles scattering from the edges of the upstream collimators. A few percent of the beam particles are lost here. After the deflection of the beams into the Arcs, primary and secondary energy collimation is performed, with a few percent loss in particles. Collimation in the final focus removes off-energy and off-axis particles, but only about 0.1% or less of the beam is removed. Finally, the synchrotron radiation is controlled by keeping the beam angular divergences below about 300 μrad and using an elaborate set of masks in the beam vacuum chamber at both ends of the detector. Of course, collimation of both beams is needed and in practice the backgrounds for the two beams often have significantly different behaviors.

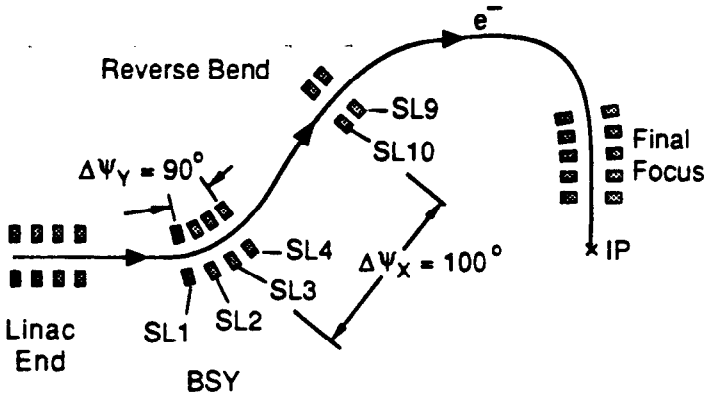

Fig. 21 Schematic view of the electron collimation system in the SLC.

9. SLC Results

The luminosity of the SLC has grown steadily during commissioning. The increase in luminosity follows approximately an exponential curve with an e-folding time of about two to three months and is highly correlated with accelerator physics studies and new hardware. The daily integration of luminosity has likewise increased. The integrated results of the 1992 run with and without e^- polarization are shown in Fig. 22. During final collisions[26] in August 1992 with polarized electrons, a peak of 350 Z^0 equivalents per day were delivered with an average of about 1500 Z^0 per week and an IP polarization of 23%.

The number of active components in the SLC, including power supplies, klystrons, kickers, vacuum pumps, computers, controls, and instrumentation, is nearly an order of magnitude larger than that of recently built circular electron colliders. Since a very large fraction of these components must be operational in order for the accelerator to function properly, the reliability of each component must be quite high. Much effort has been spent at SLAC to provide and maintain reliable active components[27]. The reliability of SLC operations has increased to levels around 60%.

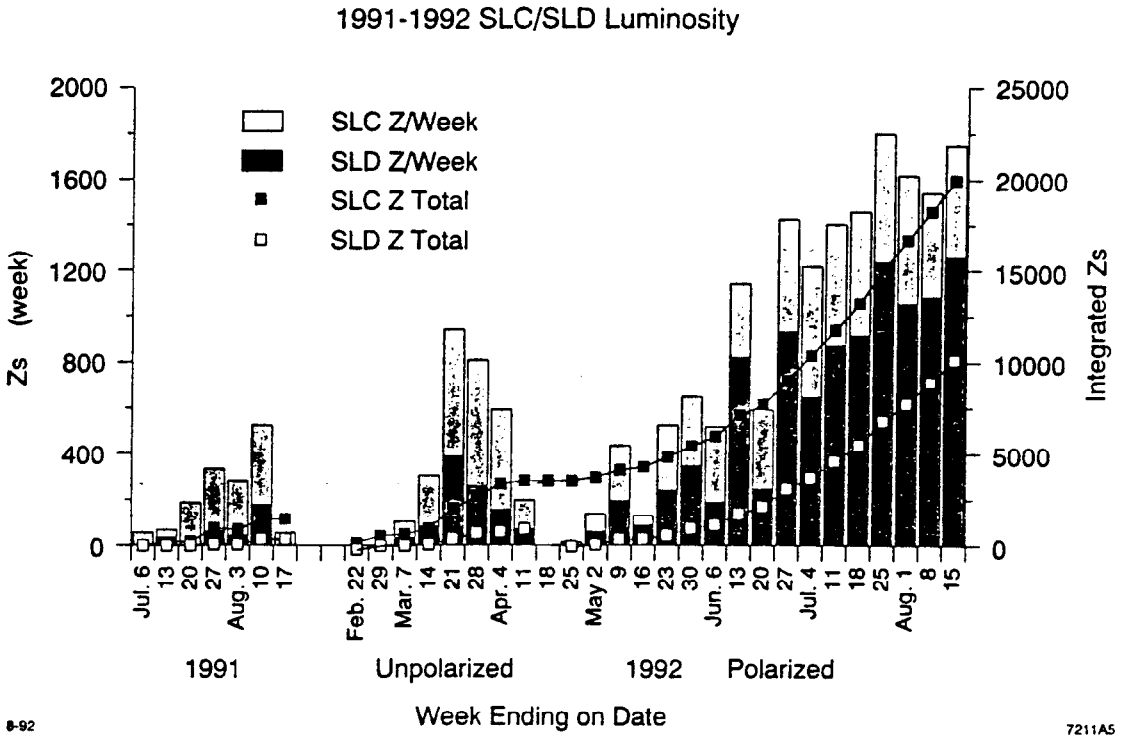

Fig. 22 Delivered Z^0 equivalents per week by the SLC to the SLD detector in 1991 and 1992. Over 350 polarized Z^0 per day have been delivered.

10. Acknowledgments

The numerous advances in accelerator and particle physics as a result of the SLC are the work of many people at the Stanford Linear Accelerator Center and from other laboratories worldwide.

11. References

1. R. Erickson, ed.,"SLC Design Handbook", Stanford (1984).
2. J. Seeman, *Annu. Rev. Nucl. Part. Sci.*, 41, p. 389-428 (1991).
3. M. Breidenbach, et al., SLAC-PUB-3798, Stanford (1985).
4. M. Breidenbach, et al., "SLC Performance in 1991", SLAC Report, Stanford (1990).
5. J. Clendenin, et al., *IEEE Trans. Nucl. Sci.* 28, p. 2452 (1981).
6. J. Clendenin, et al., SLAC-PUB-5368, Stanford (1991).
7. C. Prescott, L. Klaisner, and J. Clendenin, private communication (1992).
8. P. Corredoura, J. Judkins, and T. Limberg, private communication (1991).
9. F.-J. Decker, et al., SLAC-PUB-5747, Stanford (1992), also EPAC 1992.
10. J. Seeman, SLAC-PUB-5717, Stanford (1991) and 5th ICFA Advanced Beam Dynamics Workshop, Corpus Christi, *AIP Conf. Proc.* 255, p. 19 (1991).
11. C. Adolphsen, et al., *Proc. of IEEE USPAC*, 91CH3038-7, p. 503 (1991).
12. J. Seeman, et al., *Proc. of IEEE USPAC*, 91CH3038-7, p. 3210 (1991).
13. J. Seeman, SLAC-PUB-5716, Stanford (1991) and 5th ICFA Advanced Beam Dynamics Workshop, Corpus Christi, *AIP Conf. Proc.* 255, p. 339 (1991).
14. V. Balakin, et al., *12th Int. Conf. on High Energy Accel.*, FNAL, p. 119 (1983).
15. K. Bane, *AIP Conf. Proc.* 153, p. 971 (1987).
16. M. Ross, et al, *Proc. of IEEE USPAC*, 91CH3038-7, p. 1201 (1991).
17. J. Seeman, et al., *Proc. of IEEE USPAC*, 91CH3038-7, p. 2064 (1991).
18. J. Seeman, et al., SLAC-PUB-5705, Stanford (1992).
19. T. Himel, et al., SLAC-PUB-5470, Stanford (1991).
20. T. Barklow, et al., SLAC-PUB-5695, Stanford (1991) and 5th ICFA Advanced Beam Dynamics Workshop, Corpus Christi, *AIP Conf. Proc.* 255, p. 347 (1991).
21. N. Walker, "Relevant Experience with the SLC Final Focus", *Proc. of the Final Focus Interaction Region Workshop*, SLAC (1992).
22. K. Brown, SLAC-PUB-4811, Stanford (1988).
23. P. Bambade, et al., *Phys. Rev. Lett.* 62:2949 (1989).
24. V. Ziemann, SLAC-PUB-5595, Stanford (1991).
25. R. Jacobsen, et al., SLAC-PUB-5205, Stanford (1990).
26. N. Phinney, SLAC-PUB-5864, Stanford (1992).
27. R. Humphrey, SLAC-PUB-5708, Stanford (1992).